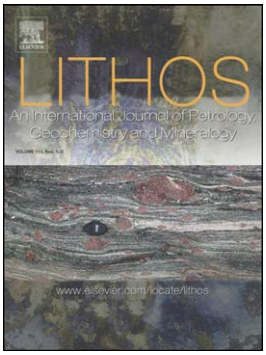

Elemental and Sr-Nd-Pb isotope geochemistry of the Cenozoic basalts in Southeast China: Insights into their mantle sources and melting processes

Pu Sun, Yaoling Niu, Pengyuan Guo, Lei Ye, Jinju Liu, Yuexing Feng

PII: S0024-4937(16)30430-3
DOI: doi:10.1016/j.lithos.2016.12.005
Reference: LITHOS 4166

To appear in: *LITHOS*

Received date: 1 July 2016
Accepted date: 2 December 2016

Please cite this article as: Sun, Pu, Niu, Yaoling, Guo, Pengyuan, Ye, Lei, Liu, Jinju, Feng, Yuexing, Elemental and Sr-Nd-Pb isotope geochemistry of the Cenozoic basalts in Southeast China: Insights into their mantle sources and melting processes, *LITHOS* (2016), doi:10.1016/j.lithos.2016.12.005

Elemental and Sr-Nd-Pb isotope geochemistry of the Cenozoic basalts in Southeast China: Insights into their mantle sources and melting processes

Pu Sun [1, 2, 3 *], Yaoling Niu [1, 2, 4, 5 **], Pengyuan Guo [1, 2], Lei Ye [6], Jinju Liu [6], Yuexing Feng [7]

[1] Institute of Oceanology, Chinese Academy of Sciences, Qingdao 266071, China

[2] Laboratory for Marine Geology, Qingdao National Laboratory for Marine Science and Technology, Qingdao 266061, China

[3] University of Chinese Academy of Sciences, Beijing 100049, China

[4] Department of Earth Sciences, Durham University, Durham DH1 3LE, UK

[5] School of Earth Science and Resources, China University of Geosciences, Beijing 100083, China

[6] School of Earth Sciences, Lanzhou University, Lanzhou 730000, China

[7] Radiogenic Isotope Facility, School of Earth Sciences, The University of Queensland, Brisbane QLD 4072, Australia

Correspondence:

* Mr. Pu Sun (pu.sun@foxmail.com)

** Professor Yaoling Niu (yaoling.niu@foxmail.com)

Abstract. We analyzed whole-rock major and trace elements and Sr-Nd-Pb isotopes

of the Cenozoic basalts in Southeast China to investigate their mantle source characteristics and melting process. These basalts are spatially associated with three extensional fault systems parallel to the coast line. After correction for the effect of olivine microlites on bulk-rock compositions and the effect of crystal fractionation, we obtained primitive melt compositions for these samples. These primitive melts show increasing SiO_2, Al_2O_3 but decreasing FeO, MgO, TiO_2, P_2O_5, CaO and CaO/Al_2O_3 from the interior to the coast. Such spatial variations of major element abundances and ratios are consistent with a combined effect of fertile source compositional variation and increasing extent and decreasing pressure of decompression melting from beneath the thick lithosphere in the interior to beneath the thin lithosphere in the coast.

These basalts are characterized by incompatible element enrichment but varying extent of isotopic depletion. This element-isotope decoupling is most consistent with recent mantle source enrichment by means of low-degree melt metasomatism that elevated incompatible element abundances without yet having adequate time for isotopic ingrowth in the mantle source regions. Furthermore, Sr and Nd isotope ratios show significant correlations with Nb/Th, Nb/La, Sr/Sr^* and Eu/Eu^*, which substantiates the presence of recycled upper continental crustal material in the mantle sources of these basalts.

Pb isotope ratios also exhibit spatial variation, increasing from the interior to the coastal area. The significant correlations of major element abundances with Pb isotope ratios indicate that the Pb isotope variations also result from varied extent and

pressure of decompression melting. We conclude that the elevated Pb isotope ratios from the interior to coast are consistent with increasing extent of decompression melting of the incompatible element depleted mantle matrix, which hosts enriched Pb isotope compositions.

Key words: SE China; Cenozoic basalts; lid effect; mantle metasomatism; recycled upper continental crust

1. Introduction

Cenozoic basaltic volcanism is widespread in eastern China (Fig. 1a). An isotopically depleted (low $^{87}Sr/^{86}Sr$ and high $^{143}Nd/^{144}Nd$), but incompatible element enriched feature has been observed in these basalts (Basu et al., 1991; Tu et al., 1991; Chung et al., 1994; Zhang et al., 1996; Zou et al., 2000; Niu, 2005; Wang et al., 2011; Huang et al., 2013). The depleted isotope signature is consistent with an asthenosphere origin. However, as the asthenospheric mantle is generally thought to be depleted in incompatible elements as inferred from the mid-ocean ridge basalts (MORB), there must be a mechanism which had re-fertilized the asthenospheric mantle source prior to the Cenozoic volcanism. Based on this inference, several models have been proposed to explain the prior enrichment, including asthenosphere-lithosphere interaction (e.g. Chung et al., 1994; Xu et al., 2005; Yan

and Zhao, 2008), involvement of recycled oceanic crust materials (Zhang et al., 2009; Wang et al., 2011) or continental crust materials (Tu et al., 1991; Liu et al., 2010; Kuritani et al., 2011) in the mantle source, which all have some difficulties (see Niu, 2005; Niu and O'Hara, 2003; Niu et al., 2012; Guo et al., 2016).

In Southeast (SE) China, the Cenozoic volcanism is spatially associated with the extensional fault systems parallel to the coastal line (Fig. 1b; Tatsumoto et al., 1992; Chung et al., 1994; Ho et al., 2003; Huang et al., 2013). Sun and Lai (1980) first noted a spatial variation in basalt compositions which tends to be more alkaline from the coast to the interior of the Fujian province (Fig. 1b). In addition, Chung et al. (1994) showed a spatial variation of Pb isotope ratios with basalts from outer Fujian having more enriched Pb isotopes. Such spatially varied basalt compositions have been attributed to variable extent of addition of the old subcontinental lithospheric mantle (SCLM; Chung et al., 1994; Zou et al., 2000). However, the old depleted Archean and Proterozoic SCLM has been largely removed in the Mesozoic (Menzies, 1993; Deng et al., 2004; Xu, 2001; Gao et al., 2002; Niu, 2005; Guo et al., 2014) with the present lithosphere being young and more enriched as inferred from geochemical and petrological studies (Griffin et al., 1998; Xu et al., 2000). Hence, further studies are needed to explain the origin of such spatial variation of basalt compositions, which may offer new perspectives on the mantle source characteristics and mantle melting processes.

In this paper, we present new data of bulk-rock major and trace elements and Sr-Nd-Pb isotopes on the Cenozoic basalts in SE China. These data, together with the

literature data, show significant spatial systematics, which allows us to conclude that 1) the basalt compositional variations reflect varying extent and pressure of decompression melting beneath SE China, and 2) within asthenosphere low-degree melt metasomatism is responsible for the incompatible element enrichment of the Cenozoic volcanism.

2. Geological setting and analytical procedures

2.1 Geological setting

Southeast Asia is generally considered as an assembly of exotic continental terranes fragmented from Gondwanaland with the amalgamation largely completed during the early Mesozoic (Lin et al., 1985; Metcalfe, 1990; Tu et al., 1991; Chung et al., 1994; Zou et al., 2000). Southeast China in the Mesozoic was characterized by an active continental margin with extensive subduction-related rhyolitic and granitic magmatisms (Jahn et al., 1990; Zhou and Li, 2000; Li et al., 2012; Niu et al., 2015). The tectonic environment was then changed from convergent to extensional as a result of westward subduction of Pacific plate or Indian-Eurasia collision (Tapponnier et al., 1986). The Cenozoic basaltic volcanism in SE China is spatially associated with the three extensional lithospheric faults (Fig. 1b). These basalts contain abundant mantle xenoliths dominated by spinel lherzolite and harzburgite with minor dunite (see Fig. 1b and Appendix B for sample locations). The Ar-Ar dating gives eruption ages of

20.2 ± 0.1Ma for samples from Jiucaidi (JC), 23.3 ± 0.3 Ma from Xiadai (XD), 9.4 ± 0.1 Ma from Xiahuqiao and Caijiawan (XH & CJ), 2.2 ± 0.1 Ma from Dangyangke and Shiheng (DY & SH) (Ho et al., 2003; Huang et al., 2013). They contain abundant olivine phenocrysts, minor clinopyroxene phenocrysts and megacrysts with the groundmass being mostly aphanitic (Fig. 2).

2.2 Analytical procedures

We crushed fresh samples to chips of ≤ 5 mm to exclude phenocrysts and xenocrysts. We also removed weathered surfaces before repeatedly washed in Milli-Q water in an ultrasonic bath, dried and grounded into powders with an agate mill in a clean environment. Bulk-rock major and trace elements were analyzed at China University of Geosciences, Beijing (CUGB). Major elements were analyzed using a Leeman Prodigy Inductively Coupled Plasma Optical Emission Spectrometer (ICP-OES) and trace elements were analyzed using an Agilent 7500a Inductively Coupled Plasma Mass Spectrometry (ICP-MS). Repeated analyses of USGS reference rock standards AGV-2, W-2, BHVO-2 and national geological standard reference materials GSR-1 and GSR-3 give analytical precision better than 15% for Ni, Co, Cr and Sc and better than 5% for all other trace elements. The analytical details are given in Song et al. (2010).

Bulk-rock Sr-Nd-Pb isotope ratios were measured using a Nu Plasma HR MC-ICP-MS at the University of Queensland. About 100 mg of rock powder was

dissolved with double distilled HNO_3 + HCl + HF at 80 °C for 48h, which was then dried and redissolved with 3 ml 2 N HNO_3 at 80 °C for 12h. 1.5 ml final sample solution was loaded onto a stack of Sr-spec, TRU-spec and Ln-spec resin columns to separate Sr, Nd and Pb, using a streamlined procedure modified after Míková and Denková (2007) and Makishima et al. (2008). The measured $^{87}Sr/^{86}Sr$ and $^{143}Nd/^{144}Nd$ isotope ratios were normalized for instrumental mass fraction using the exponential law to $^{86}Sr/^{88}Sr = 0.1194$ and $^{146}Nd/^{144}Nd = 0.7219$. Repeated analysis for NBS-987 gave $^{87}Sr/^{86}Sr = 0.710248 \pm 10$ (n = 37, 2σ). An in-house Nd standard, Ames Nd Metal, was used as an Nd isotope drift monitor. The cross-calibration of the Nd Metal against the international standard JNdi-1 gave an average $^{143}Nd/^{144}Nd = 0.511966 \pm 16$ (n = 20, 2σ). During the analysis, Nd Metal yielded a mean $^{143}Nd/^{144}Nd = 0.511967 \pm 8$ (n= 39, 2σ). Pb isotope ratios were normalized for instrumental mass fraction relative to NBS/SRM 997 $^{203}Tl/^{205}Tl = 0.41891$, which were then normalized against NBS981 (analyzed as a bracketing standard every six samples; White et al., 2000) using $^{206}Pb/^{204}Pb = 16.9410$, $^{207}Pb/^{204}Pb = 15.4944$, and $^{208}Pb/^{204}Pb = 36.7179$ (Collerson et al., 2002). See Appendix A for Sr-Nd-Pb isotope analytical results of the USGS reference material BHVO-2 and BCR-2.

3. Data and treatment

3.1 Major element compositions

The analytical data are given in Appendix B. The SE China basalts have variably high alkali contents with total alkalis ($Na_2O + K_2O$) of 2.08-7.24 wt.%. They may be termed tephrite/basanite, trachy basalt and alkali basalt (Fig. 2). They have variably high MgO contents (7-16 wt.%) and $Mg^{\#}$ (55-74), especially for those from DY with 11-16 wt.% MgO. Such high MgO is unlikely to represent the real melt compositions because the whole rock compositions must have contributions from micro phenocrysts (Fig. 3a; see discussions in Appendix C). To better study melt compositions, we corrected for the effects of olivine micro phenocrysts (see Appendix C for correction procedures and results). The correction has reduced MgO contents (5.39-11.86 wt.%) and $Mg^{\#}$ (48-67). Such correction may not be perfect, but the corrected data can effectively approximate the major element compositions of the melt represented by the groundmass without olivine micro phenocrysts. We thus use the corrected major element compositions in the following discussions.

3.2 Correction for fractionation effect to $Mg^{\#} = 72$

To explore major element characteristics of mantle processes, we further corrected these basalts for fractionation effect to $Mg^{\#} = 72$ because basaltic melts with $Mg^{\#} > 72$ are in equilibrium with mantle olivine of Fo > 89.6 (Roeder and Emslie, 1970; Niu et al., 1999, 2002; Niu and O'Hara, 2008; Humphreys and Niu, 2009; Niu et al., 2011).

Using a set of LLDs (liquid lines of decent) derived from a large data set of

MORB, Niu et al. (1999) first corrected the major element compositions of MORB samples for fractionation effect to $Mg^{\#}$ = 72. This method is conceptually and practically straightforward (see Niu et al., 1999; Niu and O'Hara, 2008). However, it is difficult to derive LLDs from continental intraplate basalts. This is because, as discussed above, in contrast with MORB glasses, bulk-rock compositions of most continental basalts cannot represent the compositions of melts but mixtures of melts and phenocrysts and because MORB are derived from low pressure depths beneath the thin lithosphere whereas continental basalts are derived from high pressure depths beneath the thickened lithosphere. In this case, following Humphreys and Niu (2009), we apply LLDs derived from Kilauea Iki Lava Lake of Hawaii OIB in our fractionation corrections. Such application is reasonable because (1) olivine, clinopyroxene and spinel are common liquidus phases for both OIB and continental basalts; (2) SE China and Hawaii have similar lithospheric thickness of ~ 80 km (Xu et al., 2000; An and Shi, 2006; Niu, 2005) and 90 km (Humphreys and Niu, 2009), respectively, which determines similar melt extraction pressures and primitive melt compositions (Niu et al., 2011) and thus similar order of appearance and proportions of liquidus phases between the SE China basalts and Hawaii OIB. The corrected data are given in Appendix D with the validity and effectiveness of the correction manifested by the total of 100.01 ± 0.16 wt.%.

As shown in Fig. 4, the major element compositions after fractionation correction show significant spatial variations, e.g., SiO_2 and Al_2O_3 increase while TiO_2, FeO, MgO, CaO, P_2O_5 and CaO/Al_2O_3 decrease from the interior to the coast.

3.3 Trace element compositions

Trace element data are given in Appendix B. Fig. 5a shows these basalts having varying extent of LREE (light rare earth elements) enrichment. The lack of an obvious negative Eu anomaly is consistent with the absence of plagioclase as the liquidus phase in these basalts. Our new samples all have OIB (oceanic island basalts)-like high $[La/Yb]_N$ ratios (12.1-40.4), which is consistent with the presence of garnet as a residual phase in the melting region. Compared with our samples, two of Niutoushan (NTS) basalts in the literature (Zou et al., 2000) show less enriched REEs.

In the primitive-mantle normalized multi-element spider diagram (Fig. 5b), our samples have trace element patterns similar to that of present-day average OIB with positive anomalies of HFSEs (high field strength elements; e.g. Nb and Ta). They show incompatible element enrichment similar to or more so than OIB. The two NTS samples show significantly low trace element abundances, which may suggest an origin from a depleted mantle source.

3.4 Sr-Nd-Pb isotopes

The Sr, Nd and Pb isotopic data are given in Appendix E. These basalts show generally depleted Sr and Nd isotope compositions with a limited range in $^{87}Sr/^{86}Sr_i$ (0.7033-0.7043), $^{143}Nd/^{144}Nd_i$ (0.51284-0.51302) and ε_{Nd} (+ 4.5 to + 7.6). They have

high $^{207}Pb/^{204}Pb_i$ (15.521-15.605) and $^{208}Pb/^{204}Pb_i$ (38.352-38.912) with intermediate $^{206}Pb/^{204}Pb_i$ (18.250-18.739). In Fig. 6a, $^{87}Sr/^{86}Sr$ and $^{143}Nd/^{144}Nd$ define a negative correlation. In Figs. 6b & c, Pb isotope ratios are positively correlated, with data points plotting above and subparallel to the NHRL (North Hemisphere Reference Line), showing an apparent Dupal anomaly (Hart, 1984). In addition, $^{206}Pb/^{204}Pb$ of our samples show no apparent correlations with $^{87}Sr/^{86}Sr$ and $^{143}Nd/^{144}Nd$ (Figs. 6d & e), which indicates different components in the mantle source regions responsible for the Pb isotopic enrichment and Sr-Nd isotopic enrichment, respectively.

As shown in Fig. 7, Pb isotope ratios spatially vary, increasing from the interior to the coast. However, $^{87}Sr/^{86}Sr$ and $^{143}Nd/^{144}Nd$ do not show such variation.

4 Discussion

4.1 The effect of lithospheric thickness on the major element compositions of the SE China basalts

Previous studies have demonstrated that major element contents in mantle melts depend on the melting pressure (Green and Ringwood, 1967; Jaques and Green, 1980; Stolper, 1980; Falloon et al., 1988; Niu, 1997, 2005; Walter, 1998; Niu et al., 2011; Green and Falloon, 2015). With decreasing melting pressure, SiO_2 (strongly), Al_2O_3 (moderately), CaO (weakly) increase, whereas MgO (strongly) and FeO (strongly to moderately) decrease. Based on the analysis of global OIB, Niu et al. (2011) further

concluded that lithospheric thickness variation, which is referred to as the lid effect, controlled the final melting pressure and geochemistry of the erupted melts. Variation in the initial depth of melting because of fertile mantle compositional variation and mantle potential temperature variation can influence the melt compositions, but these two factors must have secondary effects because they do not overshadow the effect of lithospheric thickness variation (Niu et al., 2011). Melts erupted on a thick lithosphere have geochemical characteristics consistent with a high melting pressure and low extent of decompression melting, whereas those erupted on a thin lithosphere show the reverse, i.e. a low melting pressure and high extent of decompression melting (Fig. 8).

Beneath SE China, the presence of cold stagnant Pacific plate in the mantle transition zone (410-660 km) (kárason and van der Hilst, 2000; Zhao, 2004) can preclude any possibility for hot plume materials rising from the lower mantle through mantle transition zone to the upper mantle (Niu, 2005), which avoids significant variation of mantle potential temperature and variation in the initial melting depth beneath this area. On the other hand, a thinning lithosphere from the interior to the coast of SE China has been inferred from geothermal studies (Chung et al., 1994; Xu et al., 1996; Huang and Xu, 2010) and petrological observations (e.g. the presence of garnet-facies mantle xenolith in the interior basalts and its absence in the coastal basalts may indicate a thicker lithosphere (> ~ 80 km?) beneath the interior). Therefore, the increasing Si_{72}, Al_{72} and decreasing Fe_{72}, Mg_{72} in SE China basalts from the interior to the coast (Fig. 4) is consistent with decreasing pressures of mantle

melting from beneath thick lithosphere to beneath thin lithosphere (Fig. 8). On the other hand, the abundance of incompatible element oxides such as TiO_2 and P_2O_5 in the mantle melts must decrease with increasing melting extents as a result of dilution effect (Niu et al., 2011). Thus, the decreasing Ti_{72} and P_{72} from the interior to the coast is consistent with increasing melting extent as the lithospheric thickness decreases (Fig. 8).

However, the decreasing, not increasing Ca_{72} from the interior to the coast (Fig. 4) is not consistent with a decreasing melting pressure. As CaO is weakly influenced by the melting pressure (see above), such spatially varied Ca_{72} must have been inherited from the mantle source compositions, i.e. the mantle source beneath the thin lithosphere of the coast has lower CaO content than beneath the thick lithosphere of the interior. As CaO is mainly hosted by clinopyroxene in mantle minerals, the decreasing Ca_{72} indicates a decreasing amount of modal clinopyroxene in the mantle source from the interior to the coast, which would be inherited from previous variable extent of clinopyroxene depletion.

4.2 Mantle metasomatism

4.2.1 Low-F melt metasomatism is responsible for the incompatible element enrichment in the SE China basalts

The SE China basalts are highly enriched in incompatible elements (Fig. 5). As

shown in Fig. 9, except for two samples from NTS (Zou et al., 2000), these basalts have higher $[La/Sm]_N$ (primitive mantle normalized La/Sm) of 2.6-4.3 than average OIB (~ 2.4; Sun and McDonough, 1989), reflecting a highly enriched mantle source (Niu and Batiza, 1997). Besides, they show Nb/U (41.2-120.3) similar to or higher than average OIB (47 ± 10; Hofmann et al., 1986), chondritic Nb/Ta (15.3-18.1) and super chondritic Zr/Hf (38.5-47.9; Niu, 2012; Dupuy et al., 1992). The elements in each ratio pairs have similar incompatibility during melting and these ratios thus largely reflect the source ratios (Hofmann et al., 1986; Niu and Batiza, 1997). All the above characters favor an asthenospheric mantle source extremely enriched in incompatible elements.

For decades, recycled oceanic crust has been considered as the enriched source material for OIB and intracontinental basalts (Hofmann and White, 1982; Hofmann, 1988; 1997; Chauvel et al., 1992; Cordery et al., 1997; Sobolev et al., 2000; Zhang et al., 2009; Wang et al., 2011). However, recycled oceanic crust is too depleted in incompatible elements to be the enriched component required by OIB (Niu and O'Hara, 2003; Pilet et al., 2008; Niu et al., 2012) and the SE China basalts. An alternative is that the enriched component is recycled continental crust material (Wright and White, 1987; Tu et al., 1991; Weaver, 1991; Jackson et al., 2007; Liu et al., 2010; Willbold and Stracke, 2010; Kuritani et al., 2011). However, continental crust material shows characteristic depletion in HFSEs (e.g. Nb and Ta) in contrast with relative enriched Nb (vs. Th) and Ta (vs. U) in OIB and the SE China basalts (Fig. 5b). Hence, recycled continental crust material is not a major source for OIB and

the SE China basalts (also see below).

Low-degree (low-F) melt metasomatism enriched in volatiles, alkalis and incompatible elements has long been considered significant in the origin of geochemically enriched mantle source (Halliday et al., 1995; Niu et al., 1996, 2002, 2012; Workman et al., 2004; Niu and O'Hara, 2003; Niu, 2008; Pilet et al., 2008; Guo et al., 2014, 2016). Volatiles (e.g. H_2O and CO_2) that can lower the peridotite solidus are crucial in triggering the partial melting and forming such incompatible element enriched low-F melt (Wyllie, 1980, 1987, 1988; Niu et al., 2012). Beneath eastern China, the subducted Pacific plate has been detected to lie horizontally in the mantle transition zone (410-660 km) (kúrason and van der Hilst, 2000; Zhao, 2004), which can release water as a result of thermal equilibrium with the ambient mantle (Niu, 2005, 2014). The water so released can lower the solidus of ambient mantle, form low-F melt and metasomatize the overlying asthenosphere and lithospheric mantle (Fig. 10). The metasomatic melt can exist as scattered veinlets in the surrounding depleted mantle matrix (Niu et al., 1996, 2011, 2012; Niu and O'Hara, 2003; Pilet et al., 2008). Indeed, studies on mantle xenoliths entrained in the SE China basalts have revealed a metasomatized lithospheric mantle by a volatile (H_2O and CO_2) and incompatible-element enriched silicate melt (Xu et al., 2000, 2003; Yu et al., 2006). The high Zr/Hf of these basalts is also consistent with a carbonate metasomatism in the mantle source (Dupuy et al., 1992).

As the low-F melt must have high Rb/Sr, Nd/Sm, U/Pb and Th/Pb (the element on the numerator is more incompatible than that on the denominator in each ratio pair),

it will develop time integrated radiogenic Sr and Pb and unradiogenic Nd. However, as shown in Fig. 11, the radiogenic isotope ratios (i.e., $^{87}Sr/^{86}Sr$, $^{143}Nd/^{144}Nd$, $^{207}Pb/^{204}Pb$, $^{208}Pb/^{204}Pb$) show no correlations with radioactive parent/radiogenic daughter (P/D) ratios (Rb/Sr, Sm/Nd, U/Pb, Th/Pb). Furthermore, in contrast with the significant correlations between isotopes and progressively more incompatible elements of seamount lavas from the East Pacific Rise (EPR; Niu et al., 2002) which reflects an ancient enrichment of metasomatic origin in the mantle source, the SE China basalts do not show such correlations (Fig. 12). The above characteristic is a straightforward manifestation of a recent (or "current") metasomatism without enough time for isotopic ingrowth (Zou et al., 2000; Niu, 2005; Guo et al., 2016).

4.2.2 Recycled upper continental crust (UCC) material in the mantle source

The UCC is characterized by enrichment of LILEs (large ion lithophile elements), LREEs and depletion of HFSEs (Rudnick and Gao, 2003) with radiogenic Sr and unradiogenic Nd isotopes. Therefore, involvement of UCC material in the mantle source will decrease the HFSE/LILE and HFSE/LREE ratios and $^{143}Nd/^{144}Nd$ while increase $^{87}Sr/^{86}Sr$ in the derived melt (Weaver, 1991; Jackson et al., 2007; Willbold and Stracke, 2010). As shown in Fig. 13, $^{87}Sr/^{86}Sr$ and $^{143}Nd/^{144}Nd$ show scattered but significant correlations with Nb/Th and Nb/La, which is consistent with incorporation of recycled UCC material with high $^{87}Sr/^{86}Sr$, low $^{143}Nd/^{144}Nd$, and low HFSE/LILE, HFSE/LREE ratios. Furthermore, UCC shows negative Sr and Eu anomalies (Rudnick

and Gao, 2003; Niu and O'Hara, 2009). The significant correlations of $^{87}Sr/^{86}Sr$ and $^{143}Nd/^{144}Nd$ with Sr/Sr^* and Eu/Eu^* ($Sr/Sr^* = 2\times Sr_{PM}/(Pr_{PM}+Nd_{PM})$, $Eu/Eu^* = 2\times Eu_{PM}/(Sm_{PM}+Gd_{PM})$) (Fig. 13) further confirm the contribution of recycled UCC material in the mantle source (Jackson et al., 2007). The recycled UCC material was most likely originated from subduction of terrigenous sediments along with the Pacific plate, which can melt in the mantle transition zone, mix with the Low-F melt and metasomatize the overlying asthenosphere (Zhang et al., 2007; Kuritani et al., 2011). It should be noted that although recycled UCC material can be identified in the mantle source, this material is not the actual cause for the incompatible element enrichment in the SE China basalts. This is because compared with the SE China basalts, 1) UCC material is not enriched enough in incompatible elements (Fig. 5); 2) UCC material is far too depleted in HFSEs and has low Nb/U, Nb/Ta and Zr/Hf ratios (Fig. 9; Rudnick and Gao, 2003; Niu and Batiza, 1997; Niu and O'Hara, 2003, 2009).

4.3 Explanation on the spatially varied Pb isotope compositions

Although addition of recycled UCC material in the mantle source can explain the limited variation of Sr and Nd isotopes (Fig. 13), UCC material has low U/Pb and Th/Pb ratios comparable to or slightly higher than average N-MORB and IAB but much lower than average E-MORB and OIB (see comparisons in Appendix F), which determines UCC material should have low time-integrated Pb isotope ratios and is not a reasonable component to be a Pb isotopically enriched endmember (Workman et al.,

2004). This is manifested in Figs 6b & c with the Pb isotope compositions of average GLOSS (global subducting sediment; Plank and Langmuir, 1998) plotted as an analog of the UCC material (Stracke et al., 2003; Workman et al., 2004; Jackson et al., 2007). Apparently, GLOSS or UCC material is inadequate in $^{206}Pb/^{204}Pb$ and $^{208}Pb/^{204}Pb$ to generate the isotopic signatures displayed by the SE China basalts. Furthermore, as we concluded above that the low-F melt metasomatism is too recent to produce radiogenic ingrowth, the more enriched Pb isotope compositions in these basalts are most likely inherited from the incompatible element depleted mantle matrix.

When decompression melting occurs, the metasomatic veinlets melt first because of their lower solidus temperature than the depleted mantle matrix. With continued decompression melting, the contribution of the more depleted mantle matrix increases (Niu et al., 1996, 2002, 2011; Niu and Batiza, 1997; Niu, 2005). Therefore, if the depleted mantle matrix hosts enriched Pb isotope compositions, increasing Pb isotope ratios with increasing melting extent should be observed in the SE China basalts.

In Fig. 14, $^{206}Pb/^{204}Pb$ shows scattered, but significant correlations with major element compositions, with samples having higher $^{206}Pb/^{204}Pb$ showing higher Si_{72}, Al_{72} and lower Fe_{72}, Mg_{72}, Ca_{72}, Ti_{72}, P_{72} and Ca_{72}/Al_{72}. As we discussed above, the major element compositions largely reflect variation of mantle melting pressures and extent of decompression melting. Therefore, the correlations in Fig. 14 indicate that $^{206}Pb/^{204}Pb$ in the melt increases with decreasing melting pressures (increasing Si_{72}, Al_{72} and decreasing Fe_{72}, Mg_{72}) and increasing extent of decompression melting (decreasing Ti_{72}, P_{72}), which substantiates our above inference that the depleted

mantle matrix hosts the enriched Pb isotope compositions.

Therefore, from beneath the interior to beneath the coast, the melting pressure decreases, the melting extent increases and the contribution of incompatible element depleted mantle matrix with enriched Pb isotope compositions increases (Fig. 8), which explains the increasing Pb isotope ratios from the interior to the coast (Fig. 7). Note that the absence of spatial variation of Sr and Nd isotopes (Fig. 7) likely reflects similarly depleted Sr and Nd isotope compositions between the metasomatic agent and the depleted mantle matrix.

4.4 Geodynamics for the petrogenesis of the SE China basalts

Extension-induced asthenospheric passive upwelling and decompression melting have been popularly invoked to explain the petrogenesis of the SE China basalts (Chung et al., 1994, 1997; Ho et al., 2003). However, with essentially zero "extension rate", the extension or rift in SE China (Fig. 1) cannot induce significant asthenospheric passive upwelling or melting (see Niu, 2005).

Eastern China experienced significant lithosphere thinning in the Mesozoic (Griffin et al., 1998; Gao et al., 2002; Zhang and Zheng, 2003; Niu, 2005, 2014; Zheng et al., 2006; Deng et al., 2007; Menzies et al., 2007; Niu et al., 2015), which results in a huge variation in the lithospheric thickness of Chinese continent from > 150-200 km in the west to ~ 80 km in the east (Fig. 12). Based on this observation, Niu (2005) provides a testable model for the petrogenesis of the Cenozoic basalts. As

western Pacific subduction zones are arguably the most dynamic subduction systems on Earth, the wedge suction effect will draw asthenospheric flow from beneath eastern China towards subduction zones, which in turn requires asthenospheric replenishment from beneath western thick lithosphere to beneath eastern thin lithosphere (Fig. 10). Such eastward asthenospheric flow can thus experience upwelling and decompression melting (Niu, 2014; Green and Falloon, 2015), giving rise to the widespread Cenozoic volcanism in eastern China. The extensional fault systems (Fig. 1) provided passageways for melt ascent and migration. This model is reasonable in explaining the dynamics for the petrogenesis of the SE China basalts, although more evidence is needed.

5. Conclusions

(1) After correction for the fractionation effect, the primitive melt compositions we obtained show spatial variation with increasing SiO_2, Al_2O_3 but decreasing TiO_2, FeO, MgO, P_2O_5, CaO and CaO/Al_2O_3 from the interior to the coast.

(2) SE China basalts show depleted Sr, Nd isotopes and spatially varied Pb isotopes which increase from the interior to the coast.

(3) The spatially varied major element compositions and Pb isotope ratios are consistent with a thinning lithosphere, decreasing extent and pressure of decompression melting from beneath the thick lithosphere in the interior to beneath the thin lithosphere in the coast region. The incompatible element

depleted mantle matrix is characterized by enriched Pb isotope compositions.

(4) These basalts are highly enriched in incompatible elements with high La/Sm, Nb/U, Zr/Hf, Nb/Ta ratios, suggesting their origin from an incompatible element enriched mantle source. A recent low-F melt metasomatism within the asthenospheric mantle is required to explain such enriched source signature. Water released from the stagnant Pacific plate in the mantle transition zone beneath eastern China can lower the solidus of overlying asthenosphere and produce such incompatible element enriched low-F melt.

(5) Recycled UCC materials can be identified in the mantle source, which may be originated from subducted terrigenous sediments. They can melt in the mantle transition zone, ascend and mix with the low-F melt, and metasomatize the overlying asthenosphere.

Acknowledgements

We thank Maochao Zhang, Yanan Cong, Peiqing Hu and Junping Gao for field company and sample preparation. We thank Zhenxing Hu and Meng Duan for their great help during manuscript preparation. This work was supported by the National Natural Science Foundation of China (NSFC Grants 41130314, 91014003), Chinese Academy of Sciences (Innovation Grant Y42217101L), grants from Qingdao National Laboratory for Marine Science and Technology (2015ASKJ03) and for Marine Geological process and Environment (U1606401).

References

An M. and Shi Y. (2006) Lithospheric thickness of the Chinese continent. *Phys. Earth Planet. Inter.* **159**(3), 257-266.

Basu A. R., Junwen W., Wankang H., Guanghong X. and Tatsumoto M. (1991) Major element, REE, and Pb, Nd and Sr isotopic geochemistry of Cenozoic volcanic rocks of eastern China: implications for their origin from suboceanic-type mantle reservoirs. *Earth Planet. Sci. Lett.* **105**, 149-169.

Bouvier A., Vervoort J. D. and Patchett P. J. (2008) The Lu-Hf and Sm-Nd isotopic composition of CHUR: constraints from unequilibrated chondrites and implications for the bulk composition of terrestrial planets. *Earth Planet. Sci. Lett.* **273**, 48–57.

Chauvel C., Hofmann A. W. and Vidal P. (1992) HIMU-EM: the French Polynesian connection. *Earth Planet. Sci. Lett.* **110**, 99-119.

Chung S., Sun S., Tu K., Chen C. and Lee C. (1994) Late Cenozoic basaltic volcanism around the Taiwan Strait, SE China: product of lithosphere-asthenosphere interaction during continental extension. *Chem. Geol.* **112**, 1-20.

Chung S. L., Cheng H., Jahn B., O'Reilly S.Y. and Zhu B. (1997) Major and trace element, and Sr-Nd isotope constraints on the origin of Paleogene volcanism in South China prior to the South China Sea opening. *Lithos* **40**, 203-220.

Collerson K. D., Kamber B. S. and Schoenberg R. (2002) Applications of accurate, high-precision Pb isotope ratio measurement by multi-collector ICP-MS. *Chem. Geol.* **188**, 65-83.

Cordery M. C., Davies G. F. and Campbell I. H. (1997) Genesis of flood basalts from eclogite-bearing mantle plumes, *J. Geophys. Res.* **102**, 20179–20198.

Deng J., Mo X., Zhao H., Wu Z., Luo Z. and Su S. (2004) A new model for the dynamic evolution of Chinese lithosphere: 'continental roots-plume tectonics'. *Earth-Sci. Rev.* **65**, 223-275.

Deng J., Su S., Niu Y., Liu C., Zhao G., Zhao X., Zhou S. and Wu Z. (2007) A possible model for the lithospheric thinning of North China Craton: Evidence from the Yanshanian (Jura-Cretaceous) magmatism and tectonism. *Lithos* **96**, 22-35.

Dupuy C., Liotard J. and Dostal J. (1992) Zr/Hf fractionation in intraplate basaltic rocks: carbonate metasomatism in the mantle source. *Geochim. Cosmochim. Acta* **56**, 2417-2423.

Elliott T. (2003) Tracers of the slab. *Geophys. Monogr*.**138**, 23-45.

Falloon T. J., Green D. H., Hatton C. J. and Harris K. L. (1988) Anhydrous partial melting of a fertile and depleted peridotite from 2 to 30 kb and application to basalt petrogenesis. *J. Petrol.* **29**, 1257-1282.

Gao S., Rudnick R. L., Carlson R. W., McDonough W. F. and Liu Y. (2002) Re–Os evidence for replacement of ancient mantle lithosphere beneath the North China craton. *Earth Planet. Sci. Lett.* **198**, 307-322.

Green D. H. and Falloon T. J. (2015) Mantle-derived magmas: intraplate, hot-spots and mid-ocean ridges. *Sci. Bull.* **60**, 1873-1900.

Green D. H. and Ringwood A. E. (1967) The genesis of basaltic magmas. *Contrib. Miner. Petrol.* **15**, 103-190.

Griffin W. L., Andi Z., O'reilly S. Y. and Ryan C. G. (1998) Phanerozoic evolution of the lithosphere beneath the Sino-Korean craton. *Mantle dynamics and plate interactions in East Asia* **27**, 107-126.

Guo P., Niu Y., Ye L., Liu J., Sun P., Cui H., Zhang Y., Gao J., Su L. and Zhao J. (2014) Lithosphere thinning beneath west North China Craton: Evidence from geochemical and Sr-Nd-Hf isotope compositions of Jining basalts. *Lithos* **202**, 37-54.

Guo P., Niu Y., Sun P., Ye L., Liu J., Zhang Y., Feng Y.-x. and Zhao J.-x. (2016) The origin of Cenozoic basalts from central Inner Mongolia, East China: The consequence of recent mantle metasomatism genetically associated with seismically observed paleo-Pacific slab in the mantle transition zone. *Lithos* **240-243**, 104-118.

Halliday A. N., Lee D.-C., Tommasini S., Davies G. R., Paslick C. R., Fitton J. G. and James D. E. (1995) Incompatible trace elements in OIB and MORB and source enrichment in the sub-oceanic mantle. *Earth Planet. Sci. Lett.* **133**, 379-395.

Hart S. R. (1984) A large-scale isotope anomaly in the Southern Hemisphere mantle. *Nature* **309**, 753-757.

Ho K., Chen J., Lo C. and Zhao H. (2003) $^{40}Ar/^{39}Ar$ dating and geochemical characteristics of late Cenozoic basaltic rocks from the Zhejiang–Fujian region, SE China: eruption ages, magma evolution and petrogenesis. *Chem. Geol.* **197**, 287-318.

Hofmann A. W. (1988) Chemical differentiation of the Earth: the relationship between mantle, continental crust, and oceanic crust. *Earth Planet. Sci. Lett.* **90**, 297–314.

Hofmann A. W. (1997) Mantle geochemistry: The message from oceanic volcanism. *Nature*, **385**, 219-229.

Hofmann A. W. and White W. M. (1982) Mantle plumes from ancient oceanic crust. *Earth Planet. Sci. Lett.* **57**, 421-436.

Hofmann A. W., Jochum K. P., Seufert M. and White W. M. (1986) Nb and Pb in oceanic basalts: new constraints on mantle evolution. *Earth Planet. Sci. Lett.* **79**, 33-45.

Huang X. and Xu Y. (2010) Thermal state and structure of the lithosphere beneath eastern China: a synthesis on basalt-borne xenoliths. *J. Earth Sci.***21**, 711-730.

Huang X., Niu Y., Xu Y., Ma J., Qiu H. and Zhong J. (2013) Geochronology and geochemistry of Cenozoic basalts from eastern Guangdong, SE China: constraints on the lithosphere evolution beneath the northern margin of the South China Sea. *Contrib. Miner. Petrol.* **165**, 437-455.

Humphreys, E. R. and Niu Y. (2009) On the composition of ocean island basalts (OIB): The effects of lithospheric thickness variation and mantle metasomatism.

Lithos **112**(1), 118-136.

Jackson M. G., Hart S. R., Koppers A. A. P., Staudigel H., Konter J., Blusztajn J., Kurz M. and Russell J. A. (2007) The return of subducted continental crust in Samoan lavas. *Nature*, **448**(7154), 684-687.

Jahn B. M., Zhou X. H. and Li J. L. (1990) Formation and tectonic evolution of southeast China: isotopic and geochemical constraints. *Tectonophysics* **183**, 145-160.

Jaques A. L. and Green D. H. (1980) Anhydrous melting of peridotite at 0–15 kb pressure and the genesis of tholeiitic basalts. *Contrib. Miner. Petrol.* **73**, 287-310.

Kárason H. and van der Hilst R. D. (2000) Constraints on mantle convection from seismic geotomography. *Geophys. Monogr.* **121**, 277-288.

Kuritani T., Ohtani E. and Kimura J. (2011) Intensive hydration of the mantle transition zone beneath China caused by ancient slab stagnation. *Nature Geosci.* **4**(10), 713-716.

Li Z. X., Li X. H., Chung S. L., Lo C., Xu X. and Li W. (2012) Magmati switch-on and switch-off along South China continental margin since the Permian: transition from an Andean-type to a western Pacific type. *Tectonophysics* **523–535**, 271–290

Liu, Y., Gao S., Hu Z., Gao C., Zong K. and Wang D. (2010) Continental and oceanic crust recycling-induced melt–peridotite interactions in the Trans-North China Orogen: U–Pb dating, Hf isotopes and trace elements in zircons from mantle xenoliths. *J. Petrol.* **51**, 537-571.

Lin J. L., Fuller M. and Zhang W. Y. (1985) Preliminary Phanerozoic polar wander

paths for the North and South China blocks. *Nature* **313**, 444-449.

Makishima A., Nath B. N. and Nakamura E. (2008) New sequential separation procedure for Sr, Nd and Pb isotope ratio measurement in geological material using MC-ICP-MS and TIMS. *Geochemical Journal* **42**, 237-246.

Menzies M. A., Fan W. and Zhang M. (1993) Palaeozoic and Cenozoic lithoprobes and the loss of > 120 km of Archaean lithosphere, Sino-Korean craton, China. *Geological Society, London, Special Publications* **76**, 71-81.

Menzies M., Xu Y., Zhang H. and Fan W. (2007) Integration of geology, geophysics and geochemistry: a key to understanding the North China Craton. *Lithos* **96**, 1-21.

Metcalfe I. (1990) Allochthonous terrane processes in Southeast Asia. *Philos. Trans. R. Soc. London* **331**, 625-640.

Míková J. and Denková P. (2007) Modified chromatographic separation scheme for Sr and Nd isotope analysis in geological silicate samples. *Journal of Geosciences* **52**, 221-226.

Niu Y. (1997) Mantle melting and melt extraction processes beneath ocean ridges: evidence from abyssal peridotites. *J. Petrol.* **38**, 1047-1074.

Niu Y. (2005) Generation and evolution of basaltic magmas: some basic concepts and a new view on the origin of Mesozoic–Cenozoic basaltic volcanism in eastern China. *Geological Journal of China Universities* **11**, 9-46.

Niu Y. (2008) The origin of alkaline lavas. *Science* **320**, 883-884.

Niu, Y. (2012). Earth processes cause Zr–Hf and Nb–Ta fractionations, but why and

how? RSC Advances **2**, 3587-3591.

Niu Y. (2014) Geological understanding of plate tectonics: Basic concepts, illustrations, examples and new perspectives. *Global Tectonics and Metallogeny* **10**, 23-46.

Niu Y. and Batiza R. (1997) Trace element evidence from seamounts for recycled oceanic crust in the Eastern Pacific mantle. *Earth Planet. Sci. Lett.* **148**, 471-483.

Niu Y. and O'Hara M. J. (2003) Origin of ocean island basalts: A new perspective from petrology, geochemistry, and mineral physics considerations. *J. Geophys. Res.* **108**, 2209.

Niu Y. and O'Hara M. J. (2008) Global correlations of ocean ridge basalt chemistry with axial depth: a new perspective. *J. Petrol.* **49**(4), 633-664.

Niu Y. and O'Hara M. J. (2009) MORB mantle hosts the missing Eu (Sr, Nb, Ta and Ti) in the continental crust: new perspectives on crustal growth, crust–mantle differentiation and chemical structure of oceanic upper mantle. *Lithos* **112**, 1-17.

Niu Y., Waggoner D. G., Sinton J. M. and Mahoney J. J. (1996) Mantle source heterogeneity and melting processes beneath seafloor spreading centers: the East Pacific Rise, 18º-19º S. *J. Geophys. Res.* **101**, 27711-27733.

Niu Y., Collerson K. D., Batiza R., Wendt J. I. and Regelous M. (1999) Origin of enriched-type mid-ocean ridge basalt at ridges far from mantle plumes: The East Pacific Rise at 11º 20′ N. *J. Geophys. Res.* **104**(B4), 7067-7087.

Niu Y., Regelous M., Wendt I. J., Batiza R. and O′Hara. (2002) Geochemistry of near-EPR seamounts: importance of source vs. process and the origin of enriched

mantle component. *Earth Planet. Sci. Lett.* **199**, 327-345.

Niu Y., Wilson M., Humphreys E. R. and O'Hara M. J. (2011) The origin of intra-plate ocean island basalts (OIB): the lid effect and its geodynamic implications. *J. Petrol.* **52**, 1443-1468.

Niu Y., Wilson M., Humphreys E. R. and O'Hara M. J. (2012) A trace element perspective on the source of ocean island basalts (OIB) and fate of subducted ocean crust (SOC) and mantle lithosphere (SML). *Episodes* **35**, 310.

Niu Y., Liu Y., Xue Q., Shao F., Chen S., Duan M., Guo P., Gong H., Hu Y., Hu Z., Kong J., Li J., Liu J., Sun P., Sun W., Ye L., Xiao Y. and Zhang Y. (2015) Exotic origin of the Chinese continental shelf: new insights into the tectonic evolution of the western Pacific and eastern China since the Mesozoic. *Sci. Bull.* **60**, 1598-1616.

Pilet S., Baker M. B. and Stolper E. M. (2008) Metasomatized lithosphere and the origin of alkaline lavas. *Science* **320**, 916-919.

Plank T. and Langmuir C. H. (1998) The chemical composition of subducting sediment and its consequences for the crust and mantle. *Chem. Geol.* **145**, 325-394.

Roeder P. L. and Emslie R. F. (1970) Olivine-liquid equilibrium. *Contrib. Mineral. Petrol.* **29**, 275-289.

Rudnick R. and Gao S. (2003) Composition of the continental crust. *Treatise on geochemistry* **3**, 1-64.

Sobolev A. V., Hofmann A. W. and Nikogosian I. K. (2000) Recycled oceanic crust

observed in "ghost plagioclase" within the source of Mauna Loa lavas. *Nature* **404**, 986-990.

Song S., Su L., Li X., Zhang G., Niu Y. and Zhang L. (2010) Tracing the 850-Ma continental flood basalts from a piece of subducted continental crust in the North Qaidam UHPM belt, NW China. *Precam. Res.* **183**, 805-816.

Stracke A., Bizimis M. and Salters V. J. M. (2003) Recycling oceanic crust: quantitative constraints. *Geochem. Geophys. Geosyst.* **4**, 8003.

Stolper E. (1980) A phase diagram for mid-ocean ridge basalts: preliminary results and implications for petrogenesis. *Contrib. Miner. Petrol.* **74**, 13-27.

Sun S. and McDonough W. F. (1989) Chemical and isotopic systematics of oceanic basalts: implications for mantle composition and processes. *Geological Society, London, Special Publications* **42**, 313-345.

Sun W. and Lai Z. (1980) Petrochemical characteristics of Cenozoic volcanic rocks in Fujian province and its relationship to tectonics. *Geochimica* **2**,134-147 (in Chinese).

Tatsumoto M., Basu A. R., Huang W., Wang J. and Xie G. (1992) Sr, Nd, and Pb isotopes of ultramafic xenoliths in volcanic rocks of Eastern China: enriched components EMI and EMII in subcontinental lithosphere. *Earth Planet. Sci. Lett.* **113**, 107-128.

Tapponnier P., Peltzer G. and Armiro R. (1986) On the mechanics of the collision between India and Asia. In: M. P. Coward and A. C. Ries (Editors), Collision Tectonics. *Geol. Soc. London, Spec. Publ.* **19**, 115-157.

Tu K., Flower M. F., Carlson R. W., Zhang M. and Xie G. (1991) Sr, Nd, and Pb isotopic compositions of Hainan basalts (south China): implications for a subcontinental lithosphere Dupal source. *Geology* **19**, 567-569.

Walter M. J. (1998) Melting of garnet peridotite and the origin of komatiite and depleted lithosphere. *J. Petrol.* **39**, 29-60.

Wang X., Li Z., Li X., Li J., Liu Y., Long W., Zhou J. and Wang F. (2011) Temperature, pressure, and composition of the mantle source region of Late Cenozoic basalts in Hainan Island, SE Asia: a consequence of a young thermal mantle plume close to subduction zones? *J. Petrol.* **53**, 177-233.

Wang Y., Zhao Z., Zheng Y. and Zhang J. (2011) Geochemical constraints on the nature of mantle source for Cenozoic continental basalts in east-central China. *Lithos* **125**, 940-955.

Weaver B. L. (1991) The origin of ocean island basalt end-member compositions: Trace element and isotopic constraints. *Earth Planet. Sci. Lett.* **104**, 381-397.

White W. M., Albarède F. and Télouk P. (2000) High-precision analysis of Pb isotope ratios by multi-collector ICP-MS. *Chem. Geol.* **167**, 257-270.

Willbold M. and Stracke A. (2010). Formation of enriched mantle components by recycling of upper and lower continental crust. *Chem. Geol.* **276**(3), 188-197.

Wright E. and White W. M. (1987) The origin of Samoa: new evidence from Sr, Nd, and Pb isotopes. *Earth Planet. Sci. Lett.* **81**, 151-162.

Wyllie P. J. (1980) The origin of kimberlite. *J. Geophys. Res.* **85**, 6902-6910.

Wyllie P. J. (1987) Discussion of recent papers on carbonated peridotite, bearing on

mantle metasomatism and magmatism. *Earth Planet. Sci. Lett.* **82**, 391-397.

Wyllie P. J. (1988) Solidus curves, mantle plumes, and magma generation beneath Hawaii. *J. Geophys. Res.* **93**, 4171-4181.

Workman R. K., Hart S. R., Jackson M., Regelous M., Farley K. A., Blusztajn J., Kurz M. and Staudigel H. (2004) Recycled metasomatized lithosphere as the origin of the Enriched Mantle II (EM2) end-member: Evidence from the Samoan Volcanic Chain. *Geochem. Geophys. Geosyst*. **5**.

Xu X. S., O'Reilly S. Y., Zhou, X. and Griffin W. L. (1996) A xenolith-derived geotherm and the crust-mantle boundary at Qilin, southeastern China. *Lithos* **38**, 41-62.

Xu X. S., O'Reilly S. Y., Griffin W. L. and Zhou X. (2000) Genesis of young lithospheric mantle in southeastern China: an LAM-ICPMS trace element study. *J. Petrol.* **41**, 111-148.

Xu X. S., O'Reilly S. Y., Griffin W. L. and Zhou X. (2003). Enrichment of upper mantle peridotite: petrological, trace element and isotopic evidence in xenoliths from SE China. *Chem. Geol.* **198**, 163-188.

Xu Y. (2001) Thermo-tectonic destruction of the Archaean lithospheric keel beneath the Sino-Korean Craton in China: Evidence, timing and mechanism. *Physics and Chemistry of the Earth, Part A: Solid Earth and Geodesy* **26**, 747-757.

Xu, Y., Ma J., Frey F. A., Feigenson M. D. and Liu J. (2005) Role of lithosphere–asthenosphere interaction in the genesis of Quaternary alkali and tholeiitic basalts from Datong, western North China Craton. *Chem. Geol.* **224**,

247-271.

Yan J. and Zhao J. (2008) Cenozoic alkali basalts from Jingpohu, NE China: the role of lithosphere–asthenosphere interaction. *J. Asian Earth Sci.* **33**, 106-121.

Yu J., O'Reilly S. Y., Zhang M., Griffin W. and Xu X. (2006) Roles of melting and metasomatism in the formation of the lithospheric mantle beneath the Leizhou Peninsula, South China. *J. Petrol.* **47**, 355-383.

Zhang M., Tu K., Xie G. and Flower M. F. (1996) Subduction-modified subcontinental mantle in South China: trace element and isotope evidence in basalts from Hainan Island. *Chinese Journal of Geochemistry* **15**, 1-19.

Zhang H. and Zheng J. (2003) Geochemical characteristics and petrogenesis of Mesozoic basalts from the North China Craton: A case study in Fuxin, Liaoning Province. *Chin. Sci. Bull.* **48**, 924-930.

Zhang J., Zheng Y. and Zhao Z. (2009) Geochemical evidence for interaction between oceanic crust and lithospheric mantle in the origin of Cenozoic continental basalts in east-central China. *Lithos* **110**, 305-326.

Zhang M., Hu P., Niu Y. and Su S. (2007) Chemical and stable isotopic constraints on the nature and origin of volatiles in the sub-continental lithospheric mantle beneath eastern China. *Lithos* **96**, 55-66.

Zhao D. (2004) Global tomographic images of mantle plumes and subducting slabs: insight into deep Earth dynamics. *Phys. Earth Planet In.* **146**, 3-34.

Zheng J., Griffin W. L., O'Reilly S. Y., Yang J., Li T., Zhang M., Zhang R. Y. and Liou J.G. (2006) Mineral chemistry of peridotites from Paleozoic, Mesozoic and

Cenozoic lithosphere: constraints on mantle evolution beneath eastern China. *J. Petrol.* 47, 2233-2256.

Zhou X. M. and Li W. X. (2000) Origin of Late Mesozoic igneous rocks of southeastern China: implications for lithosphere subduction and underplating of mafic magma. *Tectonophysics* **326**, 269–287.

Zou H., Zindler A., Xu X. and Qi Q. (2000) Major, trace element, and Nd, Sr and Pb isotope studies of Cenozoic basalts in SE China: mantle sources, regional variations, and tectonic significance. *Chem. Geol.* **171**, 33-47.

Figure captions

Fig. 1. (a) Distribution of the Cenozoic volcanism in eastern China. (b) Locations of our samples from Southeast (SE) China. They are from three volcanic belts (dashed lines) subparallel to the coast line. Distance of each volcanic belt to the coast line is also indicated. Modified from Guo et al. (2014) and Ho et al. (2003).

Fig. 2. TAS diagram showing compositional variations of the SE China basalts.

Fig. 3. (a) Photomicrographs showing abundant olivine phenocrysts mixed in the groundmass (representing the melt composition). Hence, a correction for the olivine effect has been done to effectively use the bulk-rock compositions for petrogenesis discussions. (b) Clinopyroxene megacryst in the Jiucaidi basalts.

Fig. 4. Spatial variation of major element compositions after correction for the effects of crystal fractionation to $Mg^{\#}$ = 72 (See Niu et al., 1999; Niu and O'Hara, 2008; Humphreys and Niu, 2009). The primitive melt compositions show first-order spatial variation as a function of distance to the coast, i.e. SiO_2, Al_2O_3 increase, whereas TiO_2, FeO, MgO, P_2O_5, CaO and CaO/Al_2O_3 decrease from the interior to the coast.

Fig. 5. Chondrite-normalized REE patterns (a) and primitive mantle-normalized multiple incompatible element abundances (b). For comparison, average compositions of present-day OIB (Sun and McDonough, 1989) and bulk continental crust (BCC; Rudnick and Gao, 2003) are also plotted.

Fig. 6. Sr-Nd-Pb isotopic co-variations of the SE China basalts. Northern Hemisphere Reference Line (NHRL) is from Hart (1984). Pb isotopes show apparent Dupal character and poor correlations with Sr and Nd isotopes.

Fig. 7. The SE China basalts show systematic Pb isotope increase towards the coast, which is absent for Sr and Nd isotopes.

Fig. 8. Schematic illustration of the lid effect concept to explain the compositional spatial variations of the SE China basalts. The adiabatically upwelling mantle reaches the solidus and begins to melt at P_0. The base of the lithosphere constrains the final

depth of the melting (P_f). The vertical range of decompression (P_0 - P_f) is proportional to the extent of melting. The solid circles represent the mean pressure of melting recorded in the geochemistry of the erupted melts, hence the inverse correlation between the extent and pressure of melting. The melts erupted on the thick lithosphere in the interior show signatures of high pressure and low extent of decompression melting (low Si, Al and high Fe, Mg, P, Ti), whereas those erupted on the thin lithosphere in the coast showing the reverse, i.e. a low melting pressure and high extent of decompression melting (high Si, Al and low Fe, Mg, P, Ti). Furthermore, Ca content in the derived melt decreases with decreasing amount of modal clinopyroxene in the mantle source. Modified from Niu et al. (2011).

Fig. 9. Except for two depleted NTS basalts, these basalts show high $[La/Sm]_N$ with Nb/U similar to or higher than OIB, chondritic Nb/Ta and super chondritic Zr/Hf, which indicates a mantle source highly enriched in incompatible elements. Upper continental crust (UCC) material with low Nb/U, Nb/Ta and Zr/Hf ratios is not a suitable candidate for the incompatible element enrichment in the mantle source.

Fig. 10. The stagnant Pacific plate in the mantle transition zone (410-660 km) experiences isobaric heating and dehydration with time (Niu, 2005; Niu et al., 2015). The water so released can lower the solidus of overlying asthenospheric mantle and form low-degree (low-F) melts enriched in volatiles and incompatible elements that can refertilize (commonly termed “metasomatism”) the otherwise depleted

asthenospheric matrix (Niu et al., 1996, 2011, 2012; Niu and O'Hara, 2003). Melts from subducted UCC material can mix with the low-F melt and contribute to the metasomatism. Furthermore, in response to the wedge suction of western Pacific subduction zones (Niu, 2005), the asthenosphere will flow from beneath eastern China towards subduction zones, which in turn requires asthenospheric replenishment from beneath western thick lithosphere (> 150-200 km) to beneath eastern thin lithosphere (~ 80 km). The eastward asthenospheric flow undergoes continued passive upwelling, decompression melting and melt extraction, responsible for the Cenozoic basaltic volcanism in SE China.

Fig. 11. Sr-Nd-Pb isotope ratios show no correlations with their parent/daughter ratios (Rb/Sr, Sm/Nd, U/Pb and Th/Pb), suggesting a recent enrichment without enough time for radiogenic ingrowth.

Fig. 12. Correlation coefficients (R values; vertical axis) of Sr-Nd-Pb isotope ratios with incompatible element abundances of the SE China basalts in the order of decreasing relative incompatibility. East Pacific Rise (EPR) seamount lava data from Niu et al. (2002) are also plotted for comparison. In contrast to the significant coupling between isotopes and incompatible trace elements of EPR seamount lavas that reflects an ancient enrichment of metasomatic origin in the mantle source, the SE China basalts show the decoupling, reflecting a recent metasomatic source

enrichment.

Fig. 13. Significant correlations of $^{87}Sr/^{86}Sr$ and $^{143}Nd/^{144}Nd$ with Nb/Th, Nb/La, Sr/Sr^{*} and Eu/Eu^{*}, indicating that the Sr and Nd isotopically enriched component has low HFSE/LILE and HFSE/LREE ratios and negative Sr, Eu anomalies, which is consistent with the contribution of UCC material in the source regions of these basalts.

Fig. 14. Significant correlations of $^{206}Pb/^{204}Pb$ with abundances and ratios of major elements corrected for the fractionation effects to a constant level of $Mg^{\#} = 0.72$. As these fractionation-corrected major element compositions reflect fertile source compositions and/or varying extents and pressures of decompression melting with the varying Pb isotope ratios caused by varying extent of melting a heterogeneous source (see text for details).

Fig. 1

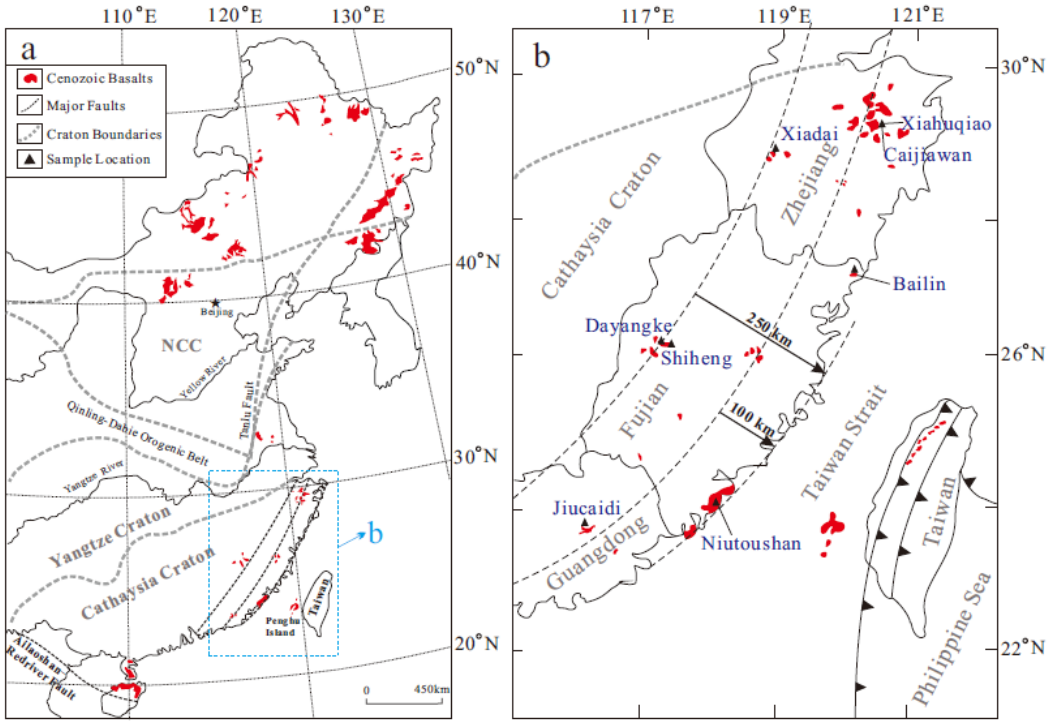

Fig. 2

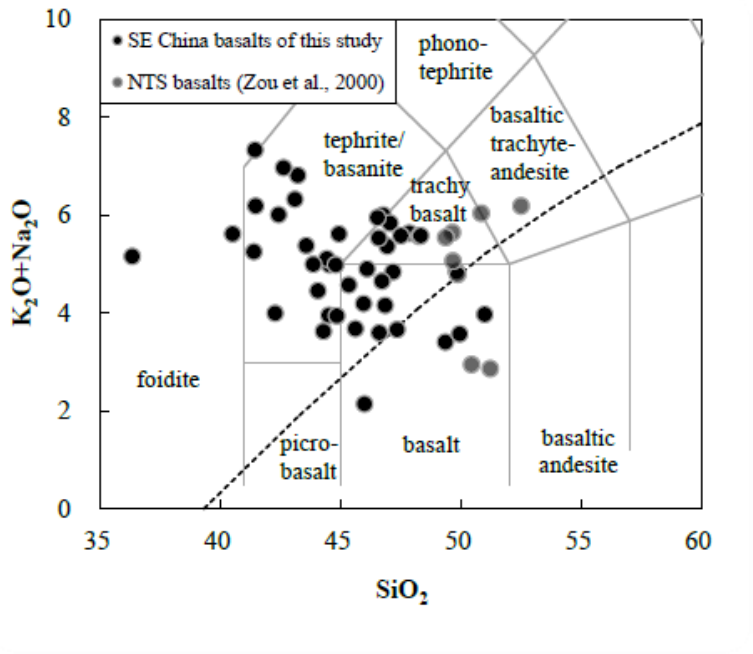

Fig. 3

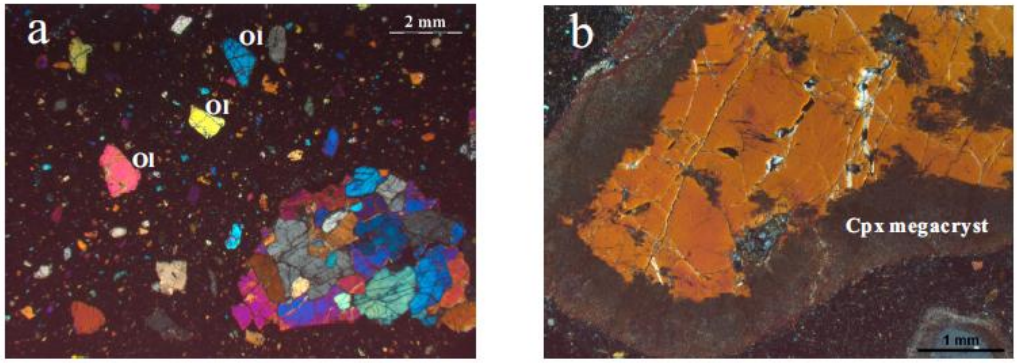

Fig. 4

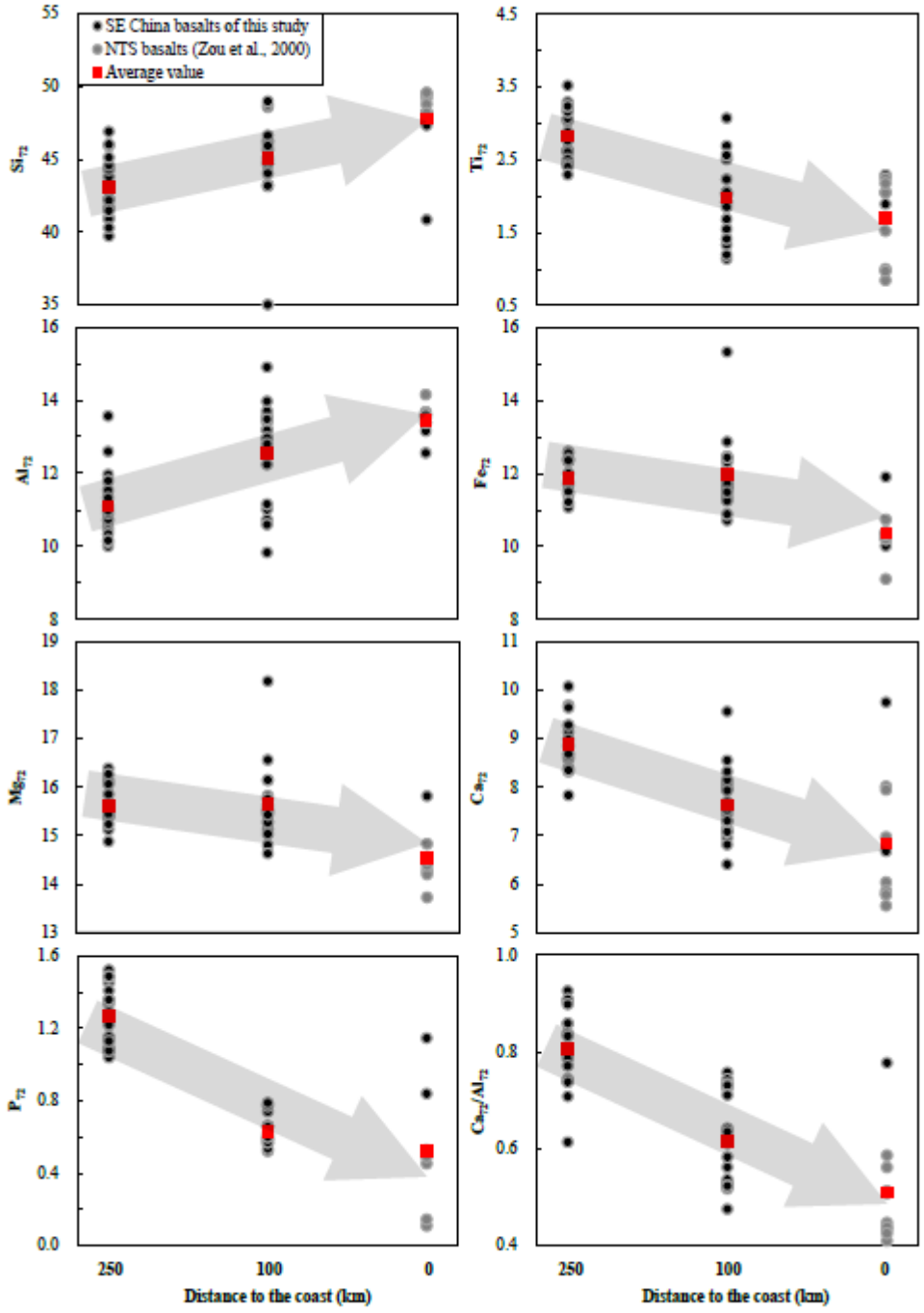

Fig. 5

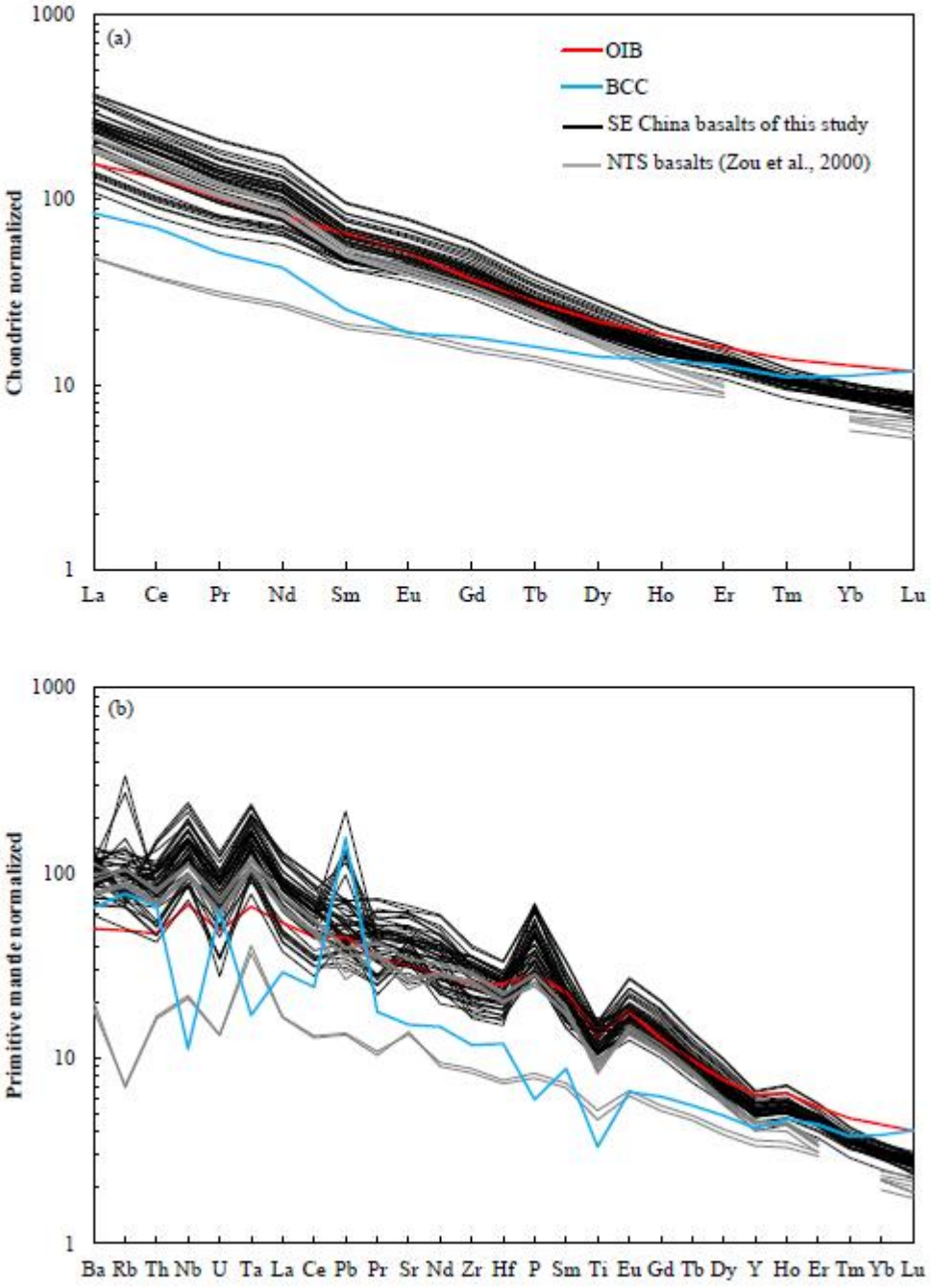

Fig. 6

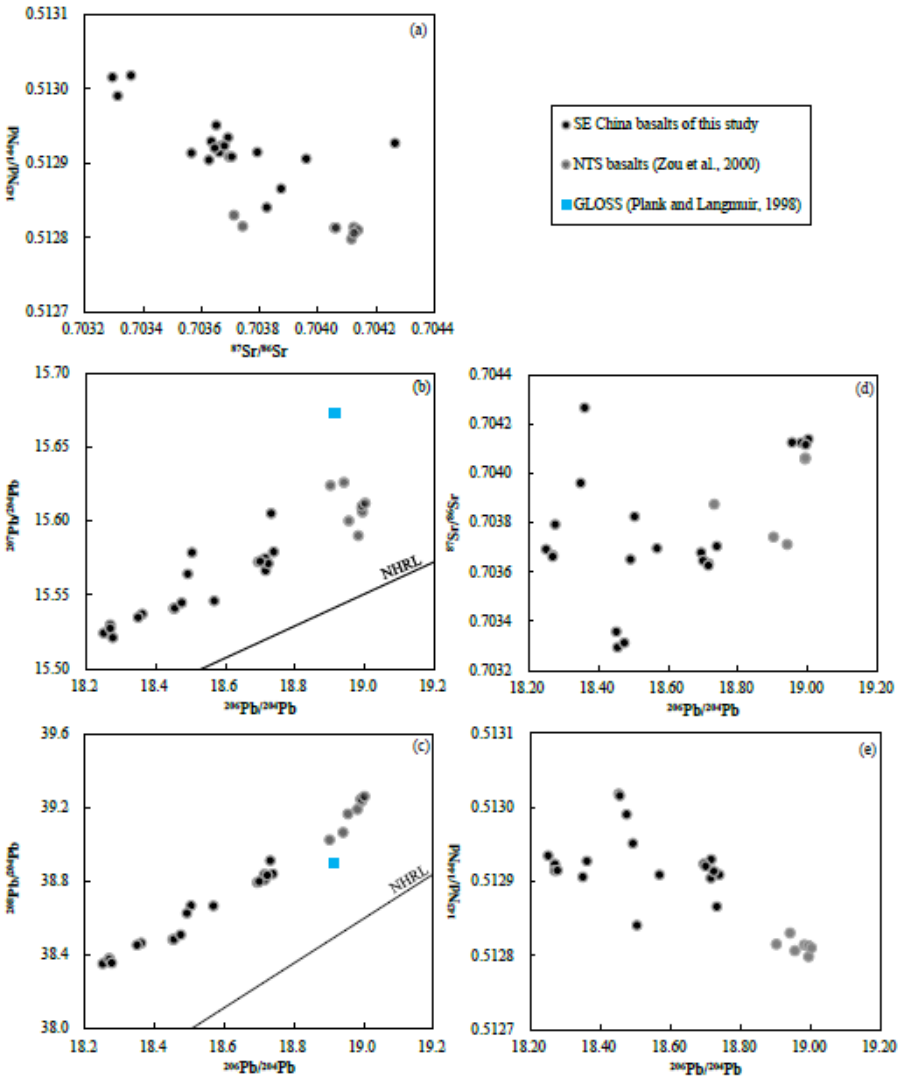

Fig. 7

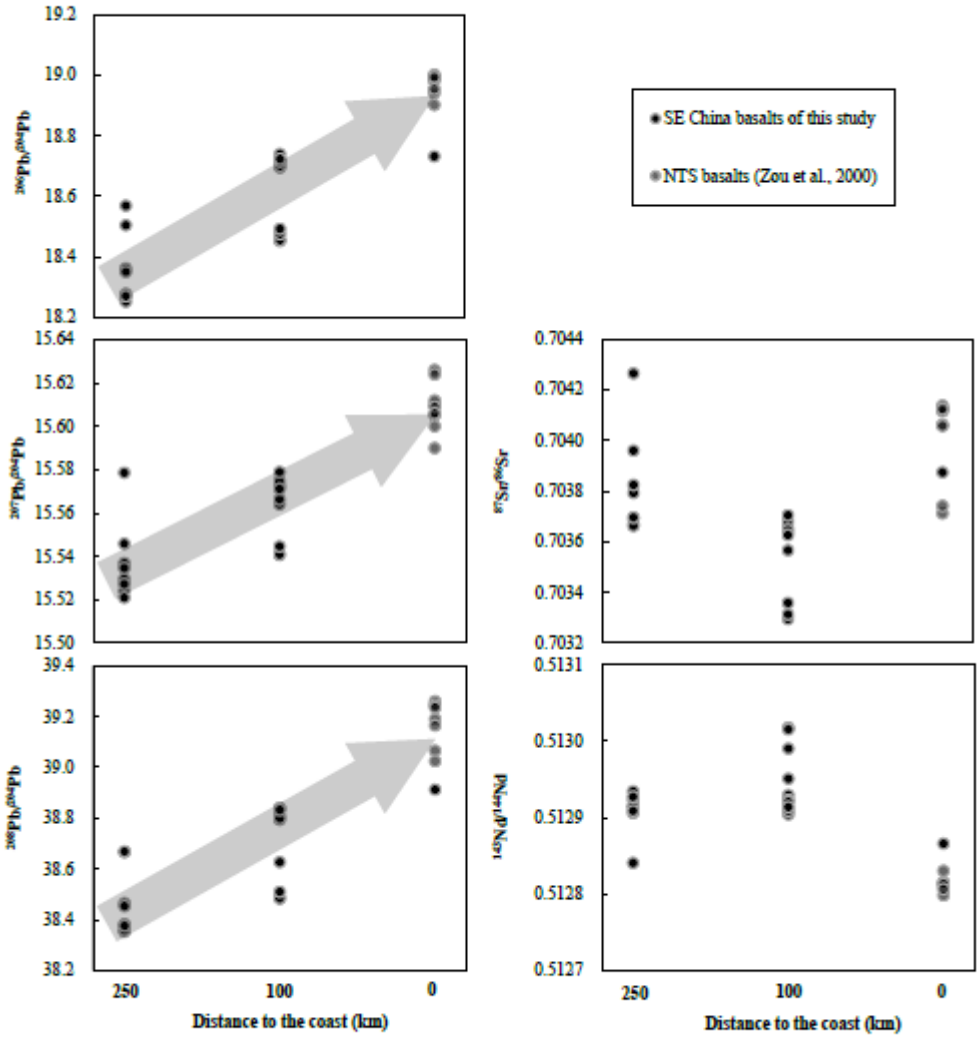

Fig. 8

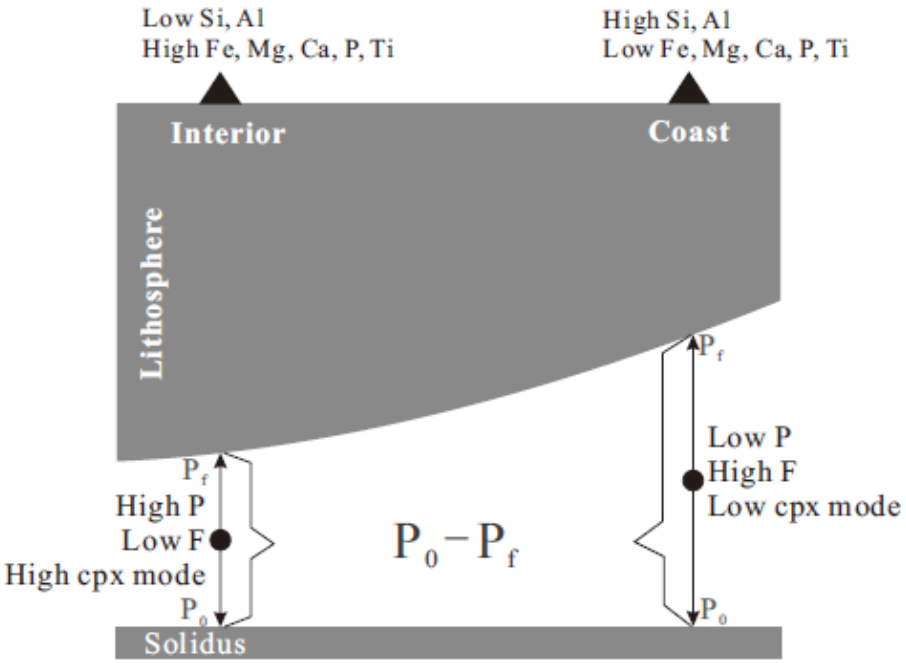

Fig. 9

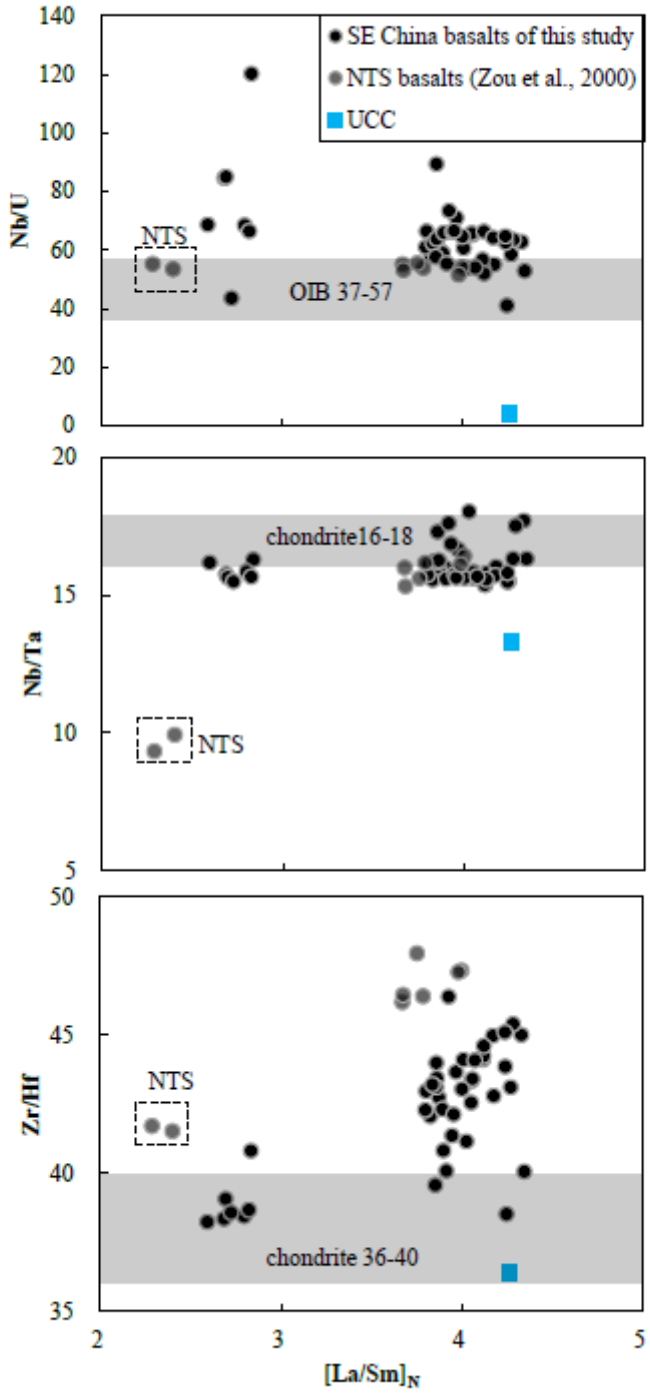

Fig. 10

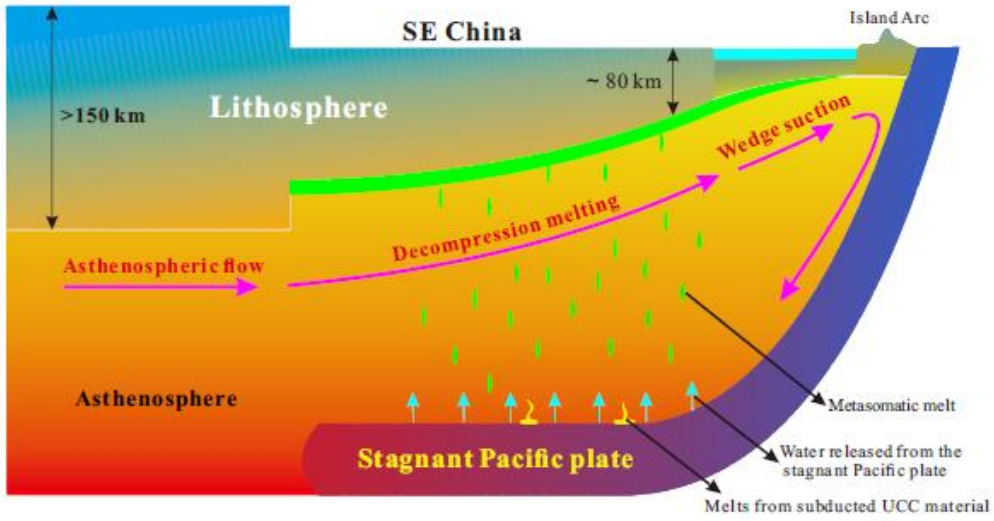

Fig. 11

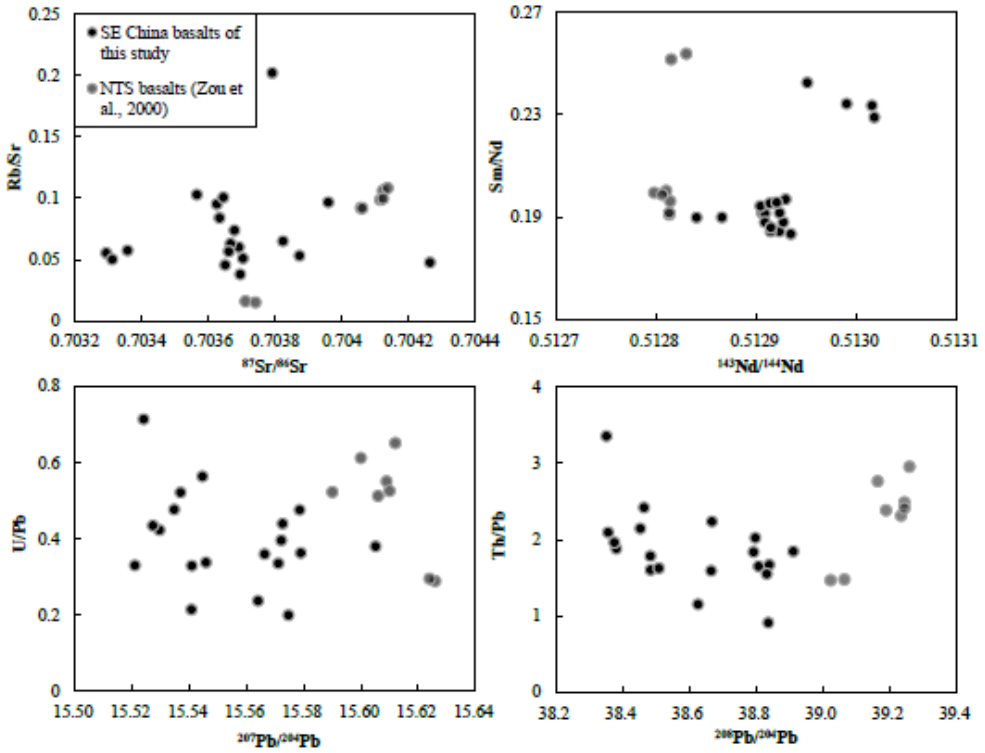

Fig. 12

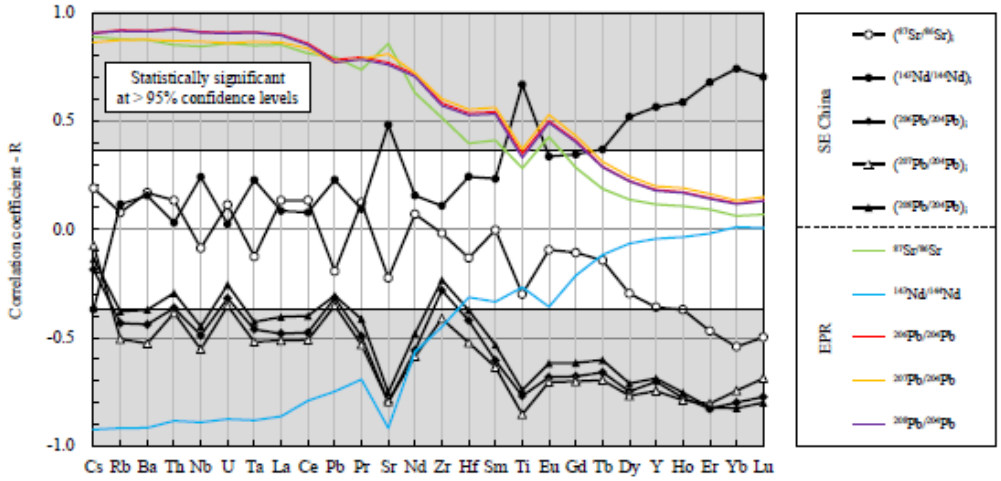

Fig. 13

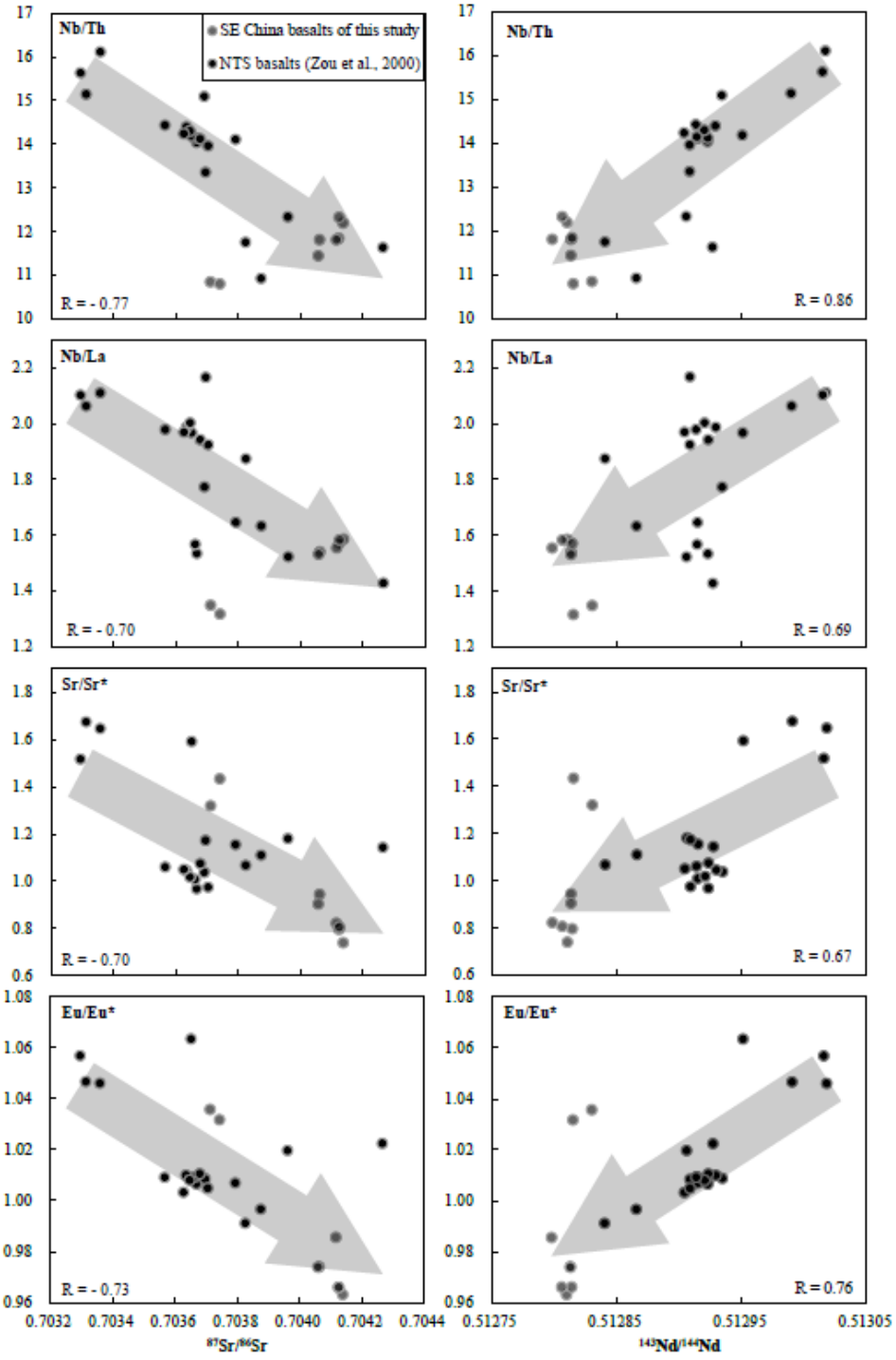

Fig. 14

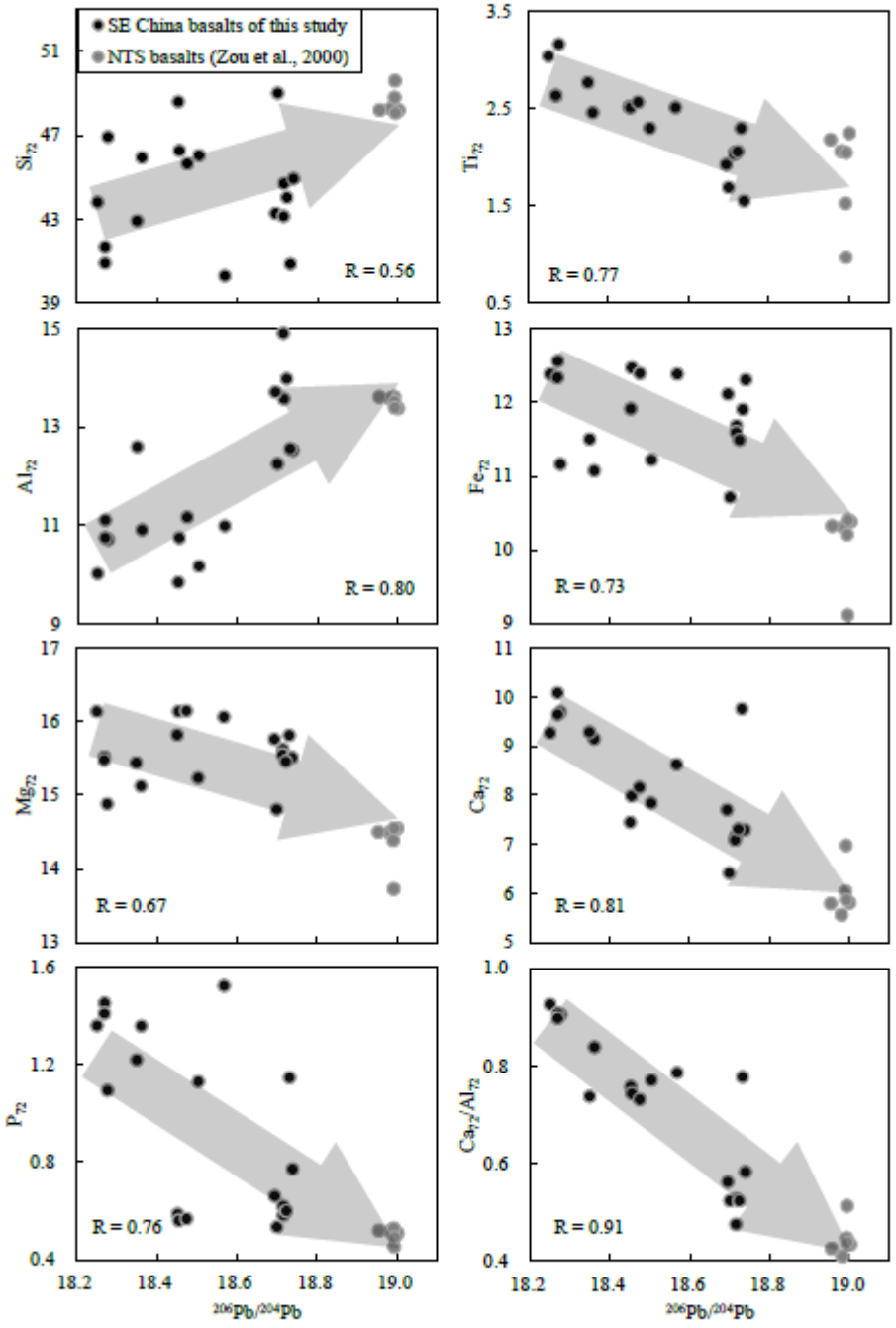

Highlights

1) The Cenozoic basalts of SE China have spatially varied major element compositions;
2) “Lid effect” can well explain the spatially varied major element compositions;
3) Mantle metasomatism explains the incompatible element enrichment in the melt;
4) Pb isotope ratios increase from the interior to the coast;
5) The depleted mantle matrix hosts enriched Pb isotope compositions.